Baku State University: Journal of Physics & Space Sciences, **2026**, v3 (2), pp. 36-53

journal homepage: http://bsuj.bsu.edu.az/en

A correlation between geomagnetic field components and aircraft accidents in civil aviation between SACs 18-24

[1]Ümit D. Göker*, [2]Ukte Aksen

[1]Astronomical Institute of the Czech Academy of Sciences, Department of Solar Physics (Former Sabbatical Fellow), Ondřejov, Czech Republic
[2]Department of Aeronautical and Astronautical Engineering, İstanbul Technical University, İstanbul, Turkey

Received 13-Mar.-2026; Accepted 28-Apr.-2026
DOI: https://doi.org/10.30546/209501.101.2026.3.02.623

Abstract

This paper extends the analysis of the relationship between geomagnetic storms (GSs) and aircraft accidents, seasonal variations, solar activity (SA), and geomagnetic activity (GA) by investigating the effects of solar wind (SW) parameters on the Earth's atmosphere and the components of the Earth's magnetic field (MF), including the D, H, and Z components, across latitudes between ±10° and ±90° in solar activity cycles (SACs) 18–24. All analyses and visualizations were performed in MATLAB R2018a, and missing data were imputed using an ARIMA forecasting model. The results indicate that aircraft accidents predominantly occurred during the decreasing phases of solar cycles (SCs), except for SAC 24. Accident frequencies were highest around equinox periods, particularly in March, September, and early October, and lowest during the solstices in June and December. During the decreasing phase of SC 19, fewer accidents occurred than in SC 18 despite stronger MF fluctuations, whereas SC 20 exhibited stable MF behavior with a higher number of accidents. Significant increases and fluctuations in MF components during the decreasing phases of SCs 22 and 23 were directly proportional to accident numbers, while SAC 24 showed minimal variability. SW parameters also varied across cycles, with plasma velocity, pressure, temperature, and beta values showing cycle-dependent behavior. The Bz-component exerted the strongest influence on Earth, while the Hn parameter after SC 21 dominated magnetospheric variations. Overall, the findings suggest that GSs alone cannot explain aircraft accidents; instead, their effects are amplified or weakened by temporal changes in the Earth's magnetic field, making them more influential during specific seasons and phases of SA.

*Corresponding author – Tel.: (+90) 501 318 18 48
e-mail address: udenizg@gmail.com; *ORCID ID*: 0000-0001-9985-5735.

Keywords: Aircraft Accidents; Geomagnetic Field Components; Geomagnetic Storm; Interplanetary Magnetic Field; Magnetosphere; Solar Wind
PACS Numbers: 94.20.-y, 94.30.Lr, 96.60.Q-, 94.05.Sd, 92.60.hv, 89.40.Dd

1. Introduction

The variable physical conditions in the solar interior, solar atmosphere, and solar wind (SW) impact the solar-terrestrial environment, which refers to the regions of the Earth's atmosphere, ionosphere, and magnetosphere. Dark regions with open magnetic field (MF) lines known as coronal holes (CHs) stream outward directly with the SW velocity between 400 km/s and 800 km/s. In contrast, huge erupting bubbles known as coronal mass ejections (CMEs) spread ahead of the erupting filaments, prominences, or large solar flares and disturb the solar-terrestrial environment at scheduled times [1]. The highest values of SW at the Earth's orbit are observed during the decreasing phase of the solar cycle (SC) when high-speed streams (HSS) that compress the ambient slow SW plasma and magnetic field (MF) throughout the interplanetary space, from the equatorward extensions of polar CHs, extend to low heliographic latitudes [2]. A weak MF of a few nT near the Earth is embedded in the SW plasma, oriented nearly parallel to the ecliptic plane, which is defined by the plane of Earth's orbit around the Sun [1]. HSS from polar CHs reaches the ecliptic plane closer to equinoxes because of the 7.2° annual variation of the Earth's heliographic latitude. During solar minima, the SW speed is systematically lower during solstices than equinoxes [2].

The change in the Sun's activity, known as "geoeffective processes", causes disturbances in the magnetosphere-ionosphere, and 11-year and 22-year SACs are well-known effects of this change [3]. The dynamic SW-magnetosphere coupling gives rise to dynamic changes in geomagnetic activities such as geomagnetic storms (GSs) and substorms, with typical durations of days and hours, respectively. These space-weather phenomena can affect satellites, navigation, telecommunications, power transmission lines, gas pipelines, the safety of astronauts and airline passengers, and the space climate, depending on long-term trends in solar variability [1]. The geospace environment, particularly the ionosphere and magnetosphere, is a multi-scale complex system exhibiting variability over a wide range of temporal and spatial scales. Because of the SW-magnetosphere-ionosphere interaction, several induced phenomena take place, such as aurorae, GSs, magnetospheric substorms, and ground geomagnetically induced currents. These are responsible for changes in the space weather conditions around Earth, i.e., the dynamic state of the near-Earth geospace environment [4]. During GSs, the SW plasma carries the MF from the interplanetary medium to the orbit of the Earth. The variation of the Earth's and Sun's MFs may change at certain times [5], and the geometry of the MF also varies with the three elements of the Earth, as D, H, and z.

The main problem we highlight in this study is that, despite numerous aircraft accidents having been attributed to various errors in the past, those caused by GSs have consistently been overlooked. We wanted to emphasize the importance of this issue, and we also identified in our study that GSs alone cannot be effective on aircraft accidents, and that the changing components of the Earth's MF during certain periods cause these storms to be more effective in some seasons and less effective in others. In this paper, data reduction for the geomagnetic field components, “D, H, and z”, is given in Section 2. Section 3 involves obtaining the data from the SW to Earth’s MF. The discussions and conclusions are given in Sections 4 and 5, respectively.

2. Data Reduction for the Geomagnetic Field Components of Earth, “D, H, and z”

We applied the accident database [6-7], which includes all civil and commercial aircraft accidents of scheduled and non-scheduled passenger airlines worldwide. The first results show that when these eruptions (e.g., CMEs and CHs) reach the Earth, the main reason for the fact that aircraft accidents are rare or non-occurring in some areas in certain periods, while they are very high in some regions, depends on the geomagnetic structure of three elements of the MF of Earth, as D, H, and z. We used 1512 aircraft accident data between February 9, 1944, and September 9, 2019. We identified and categorized them according to pilotage and mechanical reasons, bad weather conditions, turbulence, and unknown reasons that are associated with 1457 GSs. Afterward, we collected D, H, and z data from different Earth-based magnetometer observations [8]. We calibrated these different data by modification of the calibration method of the ARIMA Forecasting Model while the number density of protons (np), plasma temperature (T), plasma speed (Vp), flow pressure (P), plasma beta (β), magnetic field (B), and velocity (V) components of the SW and IMF; and northward (Hp), earthward (He), and eastward (Hn) components of the magnetosphere were taken from satellite measurements. Comparison of the monthly variation of the total number of accidents related to pilotage and mechanical reasons, bad weather conditions, turbulence, and unknown reasons, and the number of aircraft accidents for different SACs with GSs for increasing and decreasing phases of SACs 18-25 are given in Tables 1 and 2, respectively.

As seen in Table 1, the number of aircraft accidents in the decreasing phases of SACs, depending on the GS, is higher in equinox times such as March and September (and the beginning of October), with the numbers 107 (31.8%), and 85 (25.9%) (and 95 (31.5%)), respectively. In addition to this, they show lower values for the solstices in June (73 (24%)) and December (74 (19.3%)). The correlation between the predicted and actual values was found to be 97.73%, indicating a strong level of agreement.

In Table 2, in the increasing phase of the SAC, the highest number of GSs is seen in SAC 23 (111), while the highest number of GSs is seen in SAC 22 (215) in the decreasing phase. The following SACs from the highest to lowest are SAC 22 (98), SAC 20 (71), SAC 24 (68), SAC 19 (60), SAC 21 (58) and SAC 18 (36), and SAC 23 (174),

Table 1: The monthly variation of the total number of accidents relates to pilotage and mechanical reasons, bad weather conditions, turbulence, and unknown reasons, and comparison with the GSs for increasing and decreasing phases of SACs 18-25.

Month	The Total No. of Accidents (Inc. P.)	The Total No.of Accidents (Dec. P.)	The No. of GSs (Inc. P.)	The No. of GSs (Dec. P.)	The No. of Accidents by GS (Inc. P.)	The No. of Accidents by GS (Dec. P.)	* The No. of Accidents (%) (Inc. P.)	* The No. of Accidents (%) (Dec. P.)
January	238	422	45	94	56	86	23.5	20.4
February	178	296	34	69	34	72	19.1	24.3
March	239	336	54	96	54	107	22.6	31.8
April	204	262	38	67	44	72	21.6	27.5
May	178	296	44	79	46	71	25.8	24.0
June	151	304	26	77	36	73	23.8	24.0
July	179	317	50	81	50	83	27.9	26.2
August	206	320	59	83	53	83	25.7	25.9
September	200	328	49	75	50	85	25.0	25.9
October	210	302	55	91	53	95	25.2	31.5
November	215	308	41	75	46	80	21.4	26.0
December	213	383	34	68	36	74	16.9	19.3

Table 2: Comparison of the number of aircraft accidents and GSs for increasing and decreasing phases of SACs 18-25.

SACs	The Total No. of Accidents (Inc. P.)	The Total No. of Accidents (Dec. P.)	The No. of GSs (Inc. P.)	The No. of GSs (Dec. P.)	The No. of Accidents by GS (Inc. P.)	The No. of Accidents by GS (Dec. P.)	* The No. of Accidents (%) (Inc. P.)	* The No of Accidents (%) (Dec. P.)
SAC 18	497	1069	36	143	48	198	9.6	18.5
SAC 19	374	587	60	105	75	125	20.1	21.3
SAC 20	378	768	71	129	96	161	25.4	20.9
SAC 21	306	419	58	119	77	117	25.2	27.9
SAC 22	246	501	98	215	91	195	36.9	38.9
SAC 23	358	400	111	174	91	135	25.4	33.7
*SAC 24	207	130	68	70	53	50	25.6	38.5

SAC 18 (143), SAC 20 (129), SAC 21 (119), SAC 19 (105) and SAC 24 (70) in the increasing and decreasing phases of SACs, respectively. As seen from the 6th and 7th columns in Table 2, the highest number of accidents depending on GSs occurred in the decreasing phases of SACs. SAC 18 (198), SAC 22 (195), and SAC 20 (161) correspond to the increasing number of aircraft accidents. The lowest number of accidents (53 in the increasing and 50 in the decreasing) is seen in the last SC (SC 24). As seen from the 2nd and 3rd columns in Table 2, the total number of accidents increased in the decreasing phases of SACs except for SAC 24. The most striking point here is that although the total number of aircraft accidents is the lowest in the SAC 24, we see that the percentage of accidents caused by GSs is closer to other cycles.

In finding data on the Earth's geomagnetic field components, we used measurements from ground-based observatories for the years between 1944 and 2010 to find indices of GA. Most of the data in the dataset consists of daily average values obtained from observatories in Russia up to the year 2009. The data from 2010 to 2019 were sourced from other observatories, which used different calibration values. To ensure consistency across all data, values from post-2009 observatories were scaled using known reference ratios, resulting in comparable measurements. However, our graphs, that is found by new calibration techniques after the year 2010, did not give meaningful results. So, we made another estimation with the ARIMA forecasting method for the last 128 data points from 2010 to 2019. During our analysis, we mainly operate three forecast processes, such as ''Maximum Differences Forecast, Minimum Differences Forecast, and Averaged Values Forecast". A detailed explanation of the analysis technique for the reverse process with the ARIMA forecasting method is found in [9].

In Figure 1(a), the total variation of geomagnetic field components from 1944 to 2019 is shown, and we plotted the variation of geomagnetic field components for the decreasing and increasing phases of each SAC from SAC 18 to SAC 24, as shown in (b) to (h). We found from the geomagnetic field components in Figure 1 that the cycles with the greatest changes are SACs 19, 22, and 23. The cycle with the lowest change in parameters is SAC 24. The same applies to cycles 18, 20, and 21.

3. Data Acquisition and Preprocessing from the Solar Wind to Earth's Magnetic Field

3.1. Data Acquisition and Preprocessing of the Solar Wind

SW variables that can be non-Gaussian and SC dependent are observed upstream of Earth's magnetosphere in situ by satellites that are at different times at different locations and so have been shifted to a common location in the OMNI 2 data set [10]. The physical parameters in our work were taken into account from different satellites, the scalar MF strength B in nT; the MF components (Bx (GSE/GSM), By (GSM)

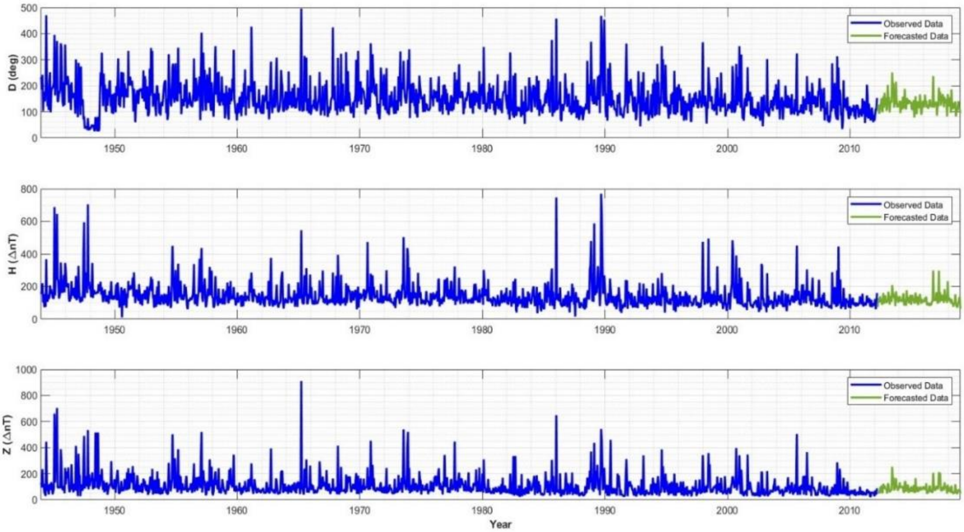

(a) Total variation of geomagnetic field components throughout the years from 1944 to 2019.

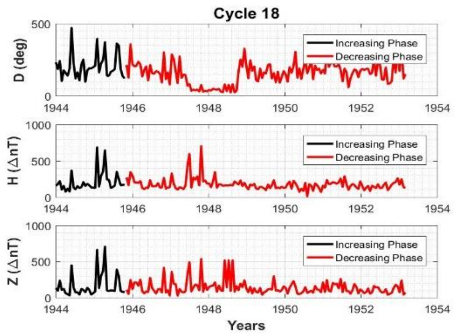

(b) The variation of geomagnetic field components for the SAC 18.

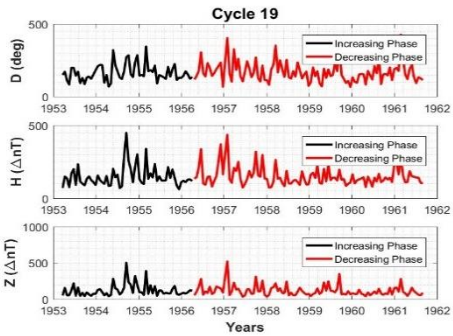

(c) The variation of geomagnetic field components for the SAC 19.

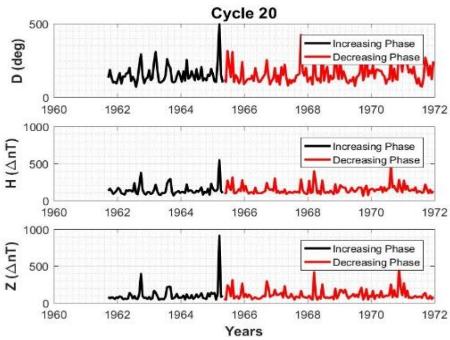

(d) The variation of geomagnetic field components for the SAC 20.

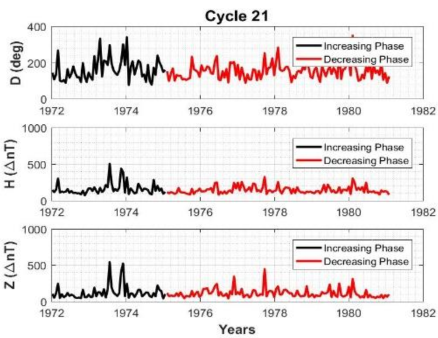

(e) The variation of geomagnetic field components for the SAC 21.

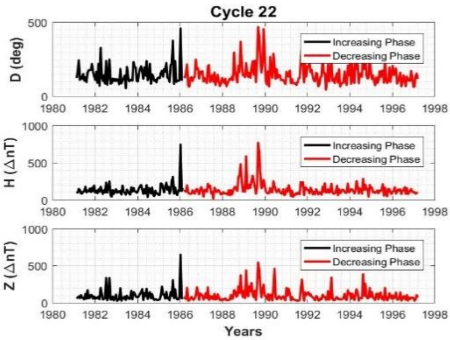

(f) The variation of geomagnetic field components for the SAC 22.

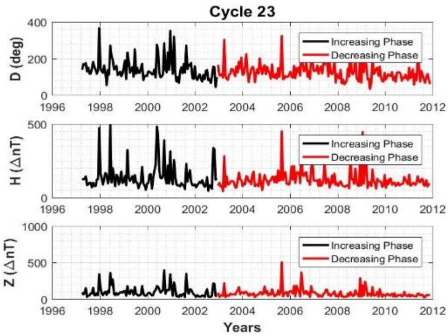

(g) The variation of geomagnetic field components for the SAC 23.

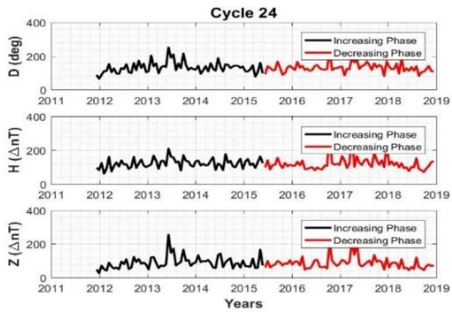

(h) The variation of geomagnetic field components for the SAC 24.

(i) We did not plot SAC 25 because the cycle has not been completed yet, and the graph will not give correct results until it is finished.

Figure 1. Variation of geomagnetic field components from the SAC 18 to SAC 24. Here, the blue lines correspond to observed data, while the green lines correspond to forecasted data in Figure (a), and the black lines correspond to the increasing phases, while the red lines correspond to the decreasing phases in Figures (b)-(h).

and Bz (GSM)) in nT; the velocity components (Vx, Vy and Vz) in km/sec; np (the number density of protons) in N/cm3, plasma temperature (T) in K, plasma speed (Vp) in km/sec, flow pressure (P) in nPa, and plasma beta (β) data are taken for the SW [11-12], and perpendicular-northward MF (Hp), earthward MF (He) and eastward MF (Hn) in Magnetosphere [13-15] for the years 1944-2019.

The data used in this paper include "Daily SW and IMF parameters" from 1963 onward, obtained from the OMNIWeb data interface provided by NASA's Goddard Space Flight Center [11] and from the National Oceanic and Atmospheric Administration (NOAA) data interface [12].

While downloading the daily-resolution data, it was observed that certain periods—especially those coinciding with GS events—contained missing values. To maintain the integrity and continuity of the time series data, missing entries were filled using daily linear interpolation. This interpolation process was performed using

MATLAB Programming Language. First, the original dataset was converted into a timetable format to enable time-aware processing. The data were then resampled to a uniform daily resolution using the retime function with linear interpolation. This approach ensured a continuous dataset with consistent daily intervals, making it suitable for further time-series analysis and statistical evaluation, as shown in Figure 2. The correlation between the predicted and actual values was found to be 98.23%, indicating a strong level of agreement.

In Figure 2(a), the total variation of geomagnetic field components throughout the years from 1944 to 2019 is given, and we plotted the variation of geomagnetic field components for the decreasing and increasing phases of each SAC from SAC 18 to SAC 24, as shown from (b) to (h). The data that corresponds to the period before 1963, the available dataset was first reordered in reverse chronological order, i.e., from the most recent date to the earliest. This step was necessary to align the structure of the data with the input requirements of the forecasting model used in the subsequent analysis. To estimate and reconstruct missing or incomplete data points beyond the observed time window, an ARIMA Forecast Modelling approach was applied. The time series was first structured into an input-output format suitable for system identification and time series modelling using the MATLAB Programming Language. An ARIMA Forecasting Model of order 90 was then trained on the reversed dataset, effectively capturing temporal dependencies based on past values. Following model estimation, a short-term forecast was performed iteratively to predict missing data. Instead of forecasting the entire missing span in a single step, the process was carried out in successive 20-step intervals. After each 20-step-ahead forecast, the predicted values were appended to the existing dataset and used as part of the input for the next forecast iteration. This stepwise forecasting strategy allowed the model to incorporate newly predicted data into subsequent training, enabling a gradual and adaptive extension of the time series. Finally, the forecasted and extended data were reordered into their original chronological sequence, resulting in a complete and temporally consistent dataset suitable for further analysis.

In Figure 2, in connection with Figure 1 in the previous section, it is evident that SW parameters also show significant changes during SACs 19, 22, and 23. The main variations in the SW, such as, the total MF started to increase in the decreasing phase of SAC 18 (from 1949s) while the β parameter shows lower values which relate to the ratio of plasma pressure to magnetic pressure, it is also in a lower value for the SAC 21; only the Vp showed smooth variation in the SAC 19, this show that the velocity of the SW is lower while the magnitude of MF is higher; only the T (as well as P) was in a lower value for the SAC 20, however, the number of aircraft accidents took place in the second order; the SACs 22, 23, and 24 showed variations in all parameters regularly, these results caused important effects for D, H, and z, however not important changes on the geomagnetic field components of Earth were seen for the SAC 24.

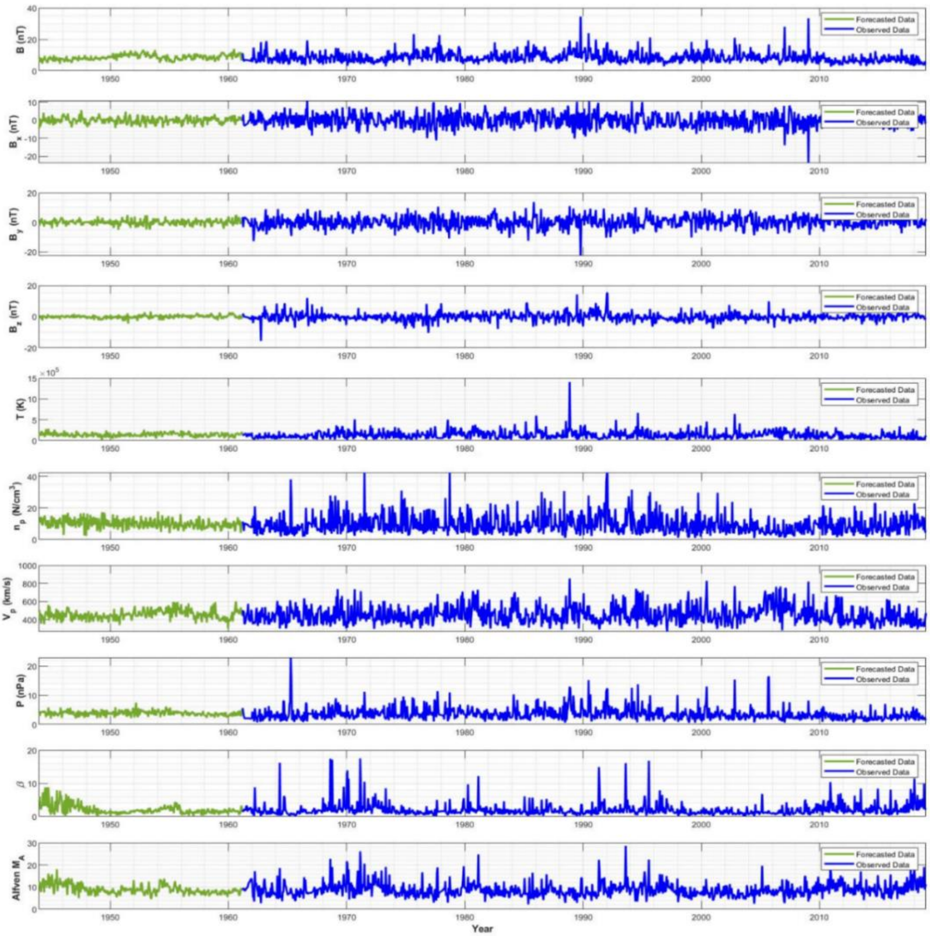

(a) Total variation of SW parameters throughout the years from 1944 to 2019.

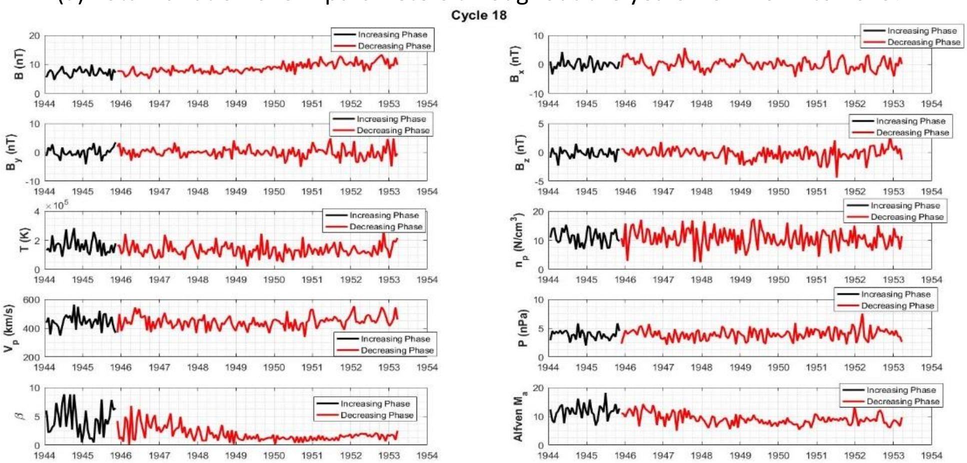

(b) The variation of SW parameters for the SAC 18.

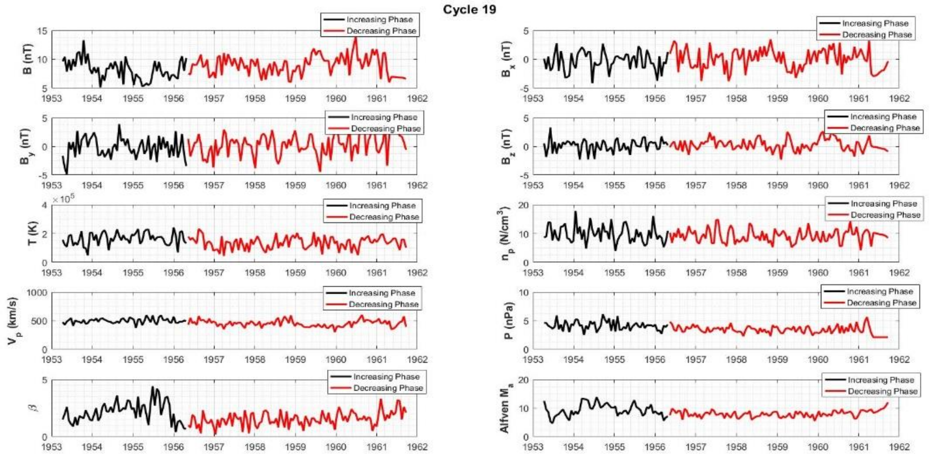

(c) The variation of SW parameters for the SAC 19.

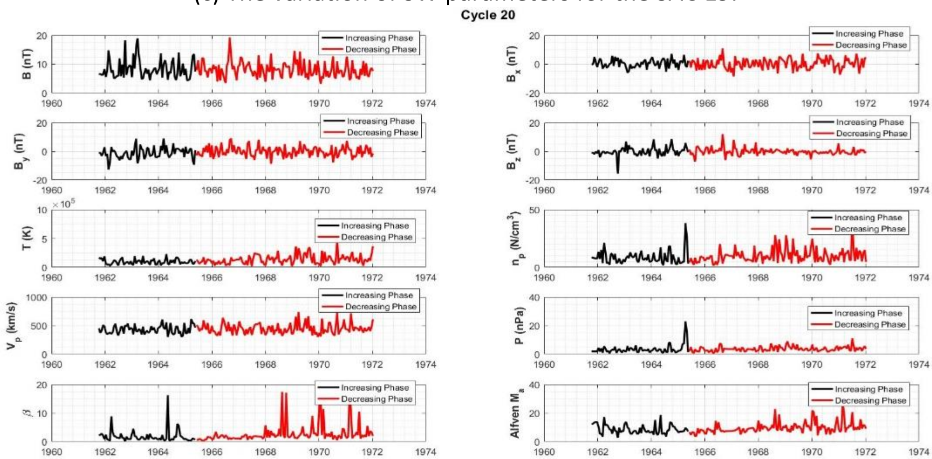

(d) The variation of SW parameters for the SAC 20.

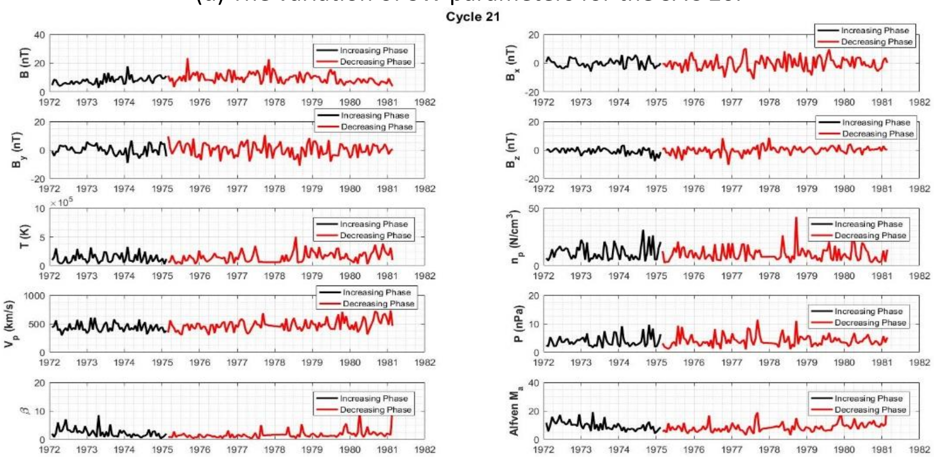

(e) The variation of SW parameters for the SAC 21.

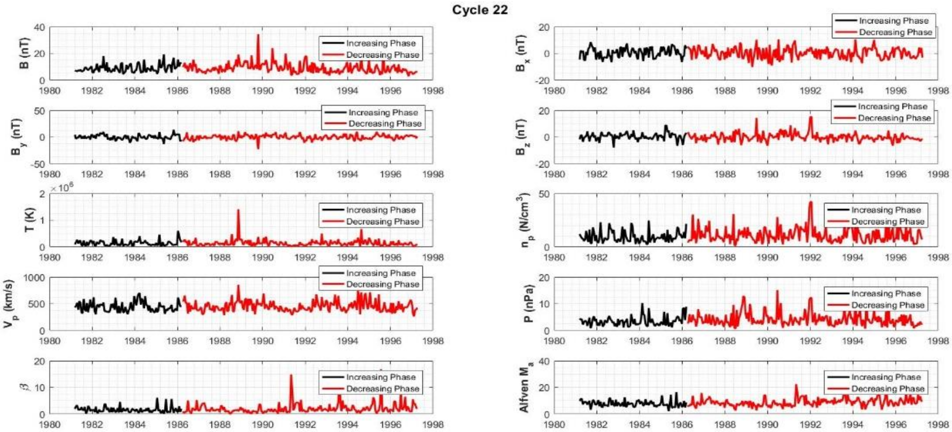

(f) The variation of SW parameters for the SAC 22.

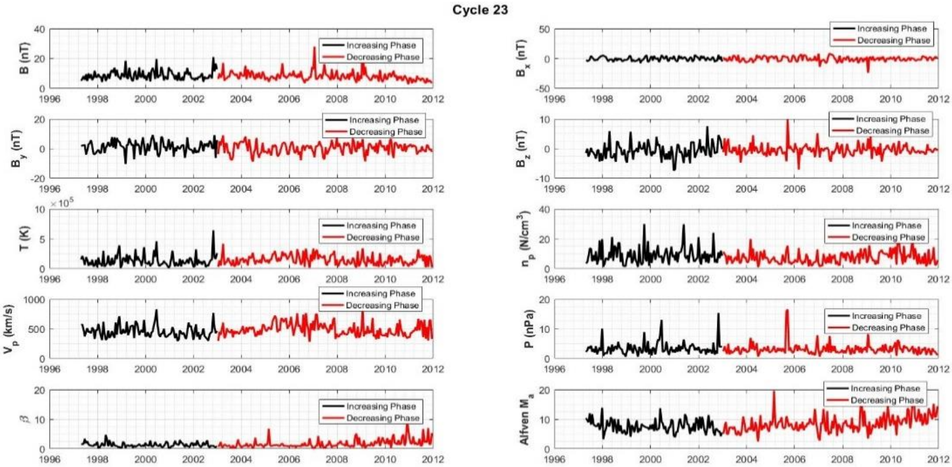

(g) The variation of SW parameters for the SAC 23.

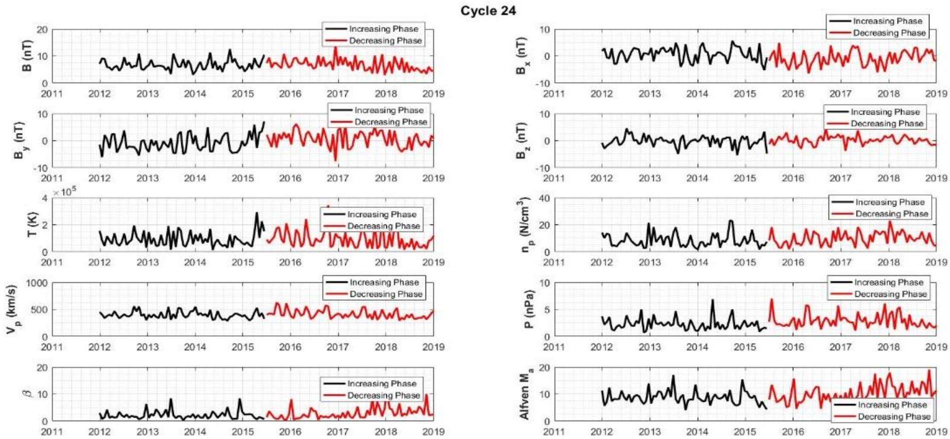

(h) The variation of SW parameters for the SAC 24

Figure 2. Variation of SW parameters from the SAC 18 to the SAC 24. Here, the blue lines correspond to observed data, while the green lines correspond to forecasted data in Figure (a), and the black lines correspond to the increasing phases, while the red lines correspond to the decreasing phases in Figures (b)-(h).

3.2. Data Acquisition and Preprocessing in the Magnetosphere

The MF data utilized in this study for the years 1974-2019 were mainly obtained from magnetometer instruments onboard the Geostationary Operational Environmental Satellites (GOES), operated by the [15] and [16]. The dataset adheres to the "GOES Space Weather" conventions and corresponds to Level 2, time-averaged data products with a temporal resolution of one minute. We also obtained data from other satellites, [13] and [14], to fill the data gaps. The components are as follows: Hp: The MF component perpendicular to the orbital plane, directed northward. This indicates the MF strength in the northward direction at the satellite's location; He: The component perpendicular to Hp, directed toward Earth. It represents the MF component pointing from the satellite toward Earth's centre; Hn: The component perpendicular to both Hp and He, directed eastward, representing the MF strength in the eastward direction. For days corresponding to GSs, relevant data points were identified and averaged to compute a single daily value for each event. In cases where daily values were missing, linear interpolation was applied to estimate them, as shown in Figure 3. Here, the total variation in the magnetosphere throughout the years from 1944 to 2019 is given, and we plotted the variation in the magnetosphere for the decreasing and increasing phases of each SAC from SAC 18 to SAC 24, as shown from (b) to (h). There were no extraordinary changes in the SCs 18 and 19, while the jump was seen for the Hn parameter in the decreasing phase of the SC 20. The correlation coefficient between predicted and actual values was found to be 98.51%, indicating a high level of agreement.

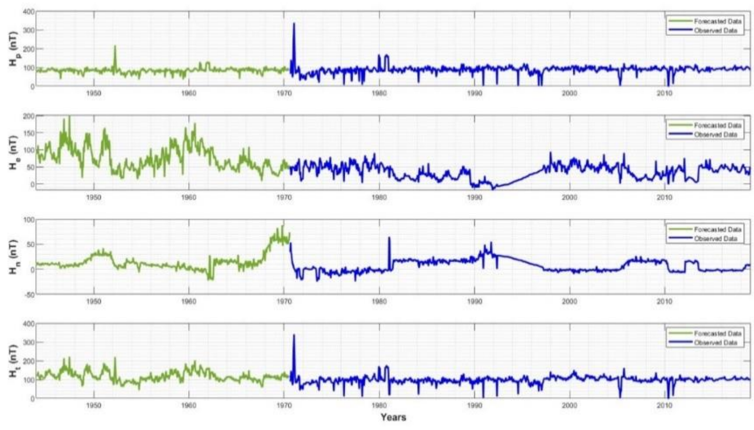

(a) Total variation in the magnetosphere components throughout the years from 1944 to 2019.

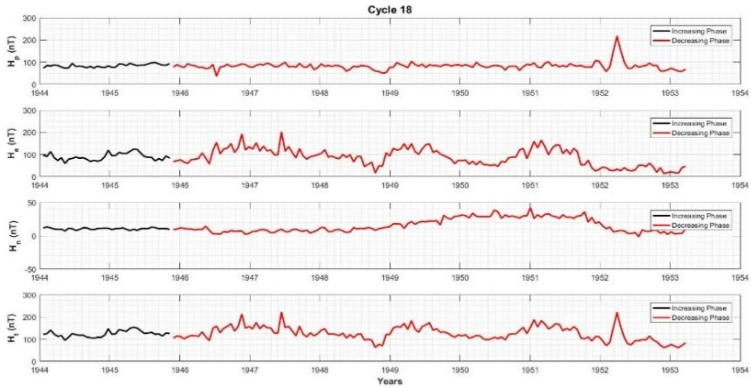

(b) The variation in the magnetosphere for the SAC 18.

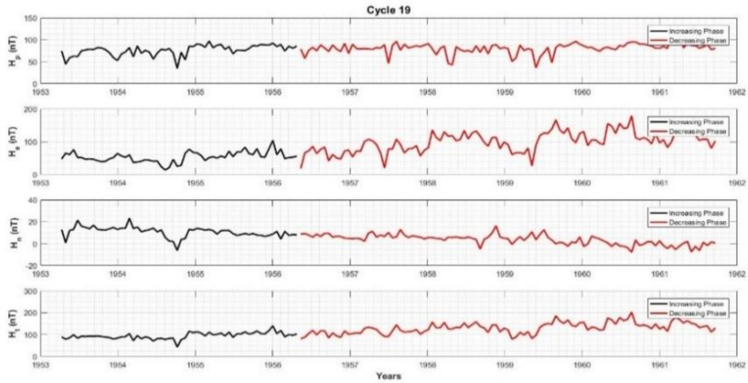

(c) The variation in the magnetosphere for the SAC 19.

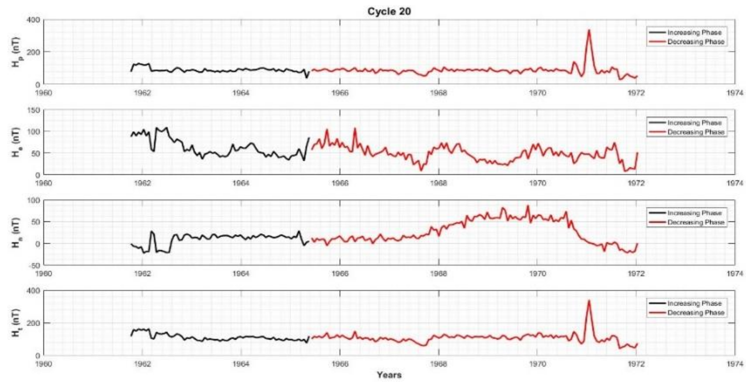

(d) The variation in the magnetosphere for the SAC 20.

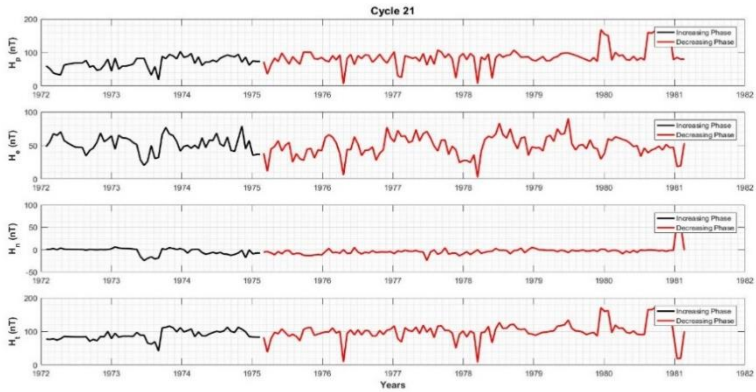

(e) The variation in the magnetosphere for the SAC 21.

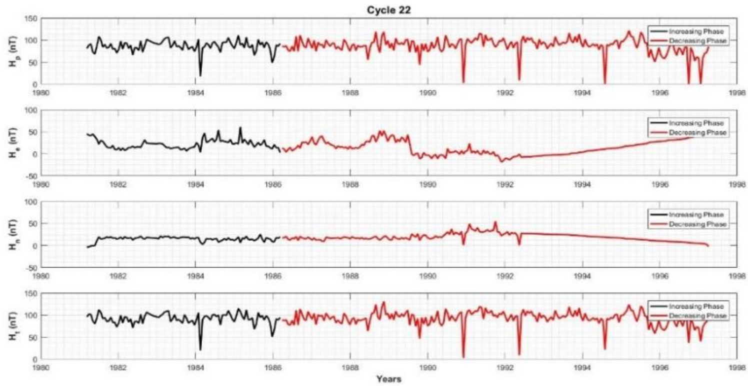

(f) The variation in the magnetosphere for the SAC 22.

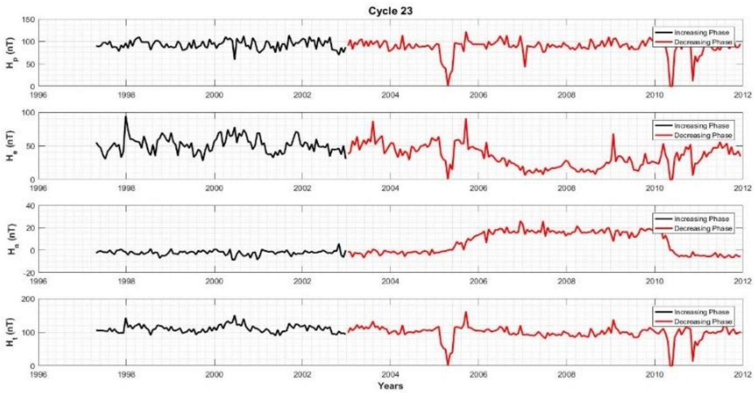

(g) The variation in the magnetosphere for the SAC 23.

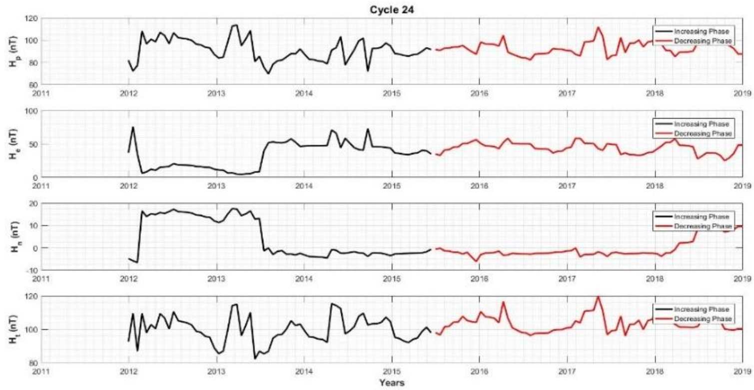

(h) The variation in the magnetosphere for the SAC 24.

Figure 3. Variation in the magnetosphere components from the SAC 18 to SAC 24. Here, the blue lines correspond to observed data, while the green lines correspond to forecasted data in Figure (a), and the black lines correspond to the increasing phases, while the red lines correspond to the decreasing phases in Figures (b)-(h).

The most significant change in all graphs was observed in Hn and He, and the quietest variation was seen in SC 21 for the Hn parameter. The number of aircraft accidents was lower in this cycle (SC 21), as well. The real abnormalities began after the SC 21; e.g., during the SC 22, no data were R e c e i v e d for nearly seven years, or there was a problem with the satellite for the He and Hn variables. The SC 24 was the cycle with the most abnormal variations in all parameters.

4. Results and Discussion

The number of aircraft accidents in the decreasing phases of SACs, depending on the GSs, was higher in the equinox times, such as March and September (and the beginning of October), with the numbers 107 (31.8%) and 85 (25.9%) (and 95(31.5%)), respectively. In addition to this, they showed lower values for the solstices in June (73(24%)) and December (74(19.3%)); in the other months, similar values followed each other as indicated in Table 1. The highest number of GSs was seen in SAC 23 (111) and SAC 22 (215) in the increasing and decreasing phases of SACs, respectively. The number of GSs following SACs from highest to lowest were SAC 22 (98), SAC 20 (71), SAC 24 (68), SAC 19 (60), SAC 21 (58), and SAC 18 (36) in the increasing phases, and SAC 23 (174), SAC 18 (143), SAC 20 (128), SAC 21 (119), SAC 19 (105), and SAC 24 (70) in the decreasing phases of SACs as seen in Table 2. The highest number of accidents, depending on GSs, occurred in the decreasing phases of SACs, and the total number of accidents increased in the decreasing phases of SACs, except for SAC 24. On the other hand, the lowest number of accidents (53 in the increasing phase and 50 in the decreasing phase) was seen in the last SC (SC 24); however, the percentage of accidents caused by GSs was closer to other cycles.

In certain periods, when high-speed SW streams and GSs (e.g., CMEs and CHs) reach the Earth, the main reason for the fact that aircraft accidents are rare or non-occurring in some areas while they are very high in some regions depends on the geomagnetic structure of the three elements of the Earth, as D, H, and z. We used 1512 aircraft accident data, and 1457 GSs corresponding to these accidents between February 9, 1944, and September 9, 2019. Afterward, we collected D, H, and z data from different Earth-based magnetometer observations and plotted these data in Figure 1. As seen in Figures 1(b)-1(h), the decreasing phase lasts much longer than the increasing phase. However, there were no extreme fluctuations in the Earth's MF components during the decreasing phase of the SC 18. In contrast, during the decreasing phase of the SC 19, even fewer aircraft accidents occurred than in the SC 18, and there were much more significant fluctuations. Similarly, during the decreasing phase of the SC 20, where more accidents occurred, a more stable change was seen. In the decreasing phase of SC 21, we are faced with parameters that were not only stable but also did not reach very high values. However, significant increases and fluctuations in the Earth's MF components have been observed during the decreasing phases of SCs 22 and 23. However, SC 24 was also the SC with the lowest number of accidents and the lowest changes related to SA.

Based on all our research on the parameters of GSs and Earth’s MF, we also wanted to see how SW parameters changed during these periods. As seen in Figures 2(b)-2(h), the most noticeable change was seen in the plasma velocity (Vp), e.g., the velocity of the SW plasma changing in almost all cycles. Accordingly, the lowest Vp was seen in the SC 19. In this cycle, the number of GSs was high, but their velocities were lower towards the interplanetary medium. Other cycles had similar velocity changes regardless of their numbers. The second most significant change was in the beta parameter (β). The lowest β value was seen in the SCs 21, 22, and 23, while the greatest changes were seen in SCs 18 and 19. This means that plasma pressure (P) was lower than the magnetic pressure, and there have been changes in magnetic pressure, e.g., MF lines. However, it can be seen in the figures that there has been more change in P for the SACs 21, 22, 23, and 24. The most stable periods in terms of P were the SCs 18, 19, and 20. The number density of protons (np) was the same for all SCs. The SW temperature (T) was at its lowest values in SCs 20 and 22. Under normal conditions, T and Vp should change proportionally to each other, but as seen here, this is not the case. This indicates that T or Vp was being altered by different parameters. The changes in the MF components depend on their directions, e.g., there were significant changes in all MF components during the SCs 19, 20, 21, and 24. In the SAC 20, the lowest changes were seen in the Bx and Bz components. In the same way, only the Bx component was lower in SC 23. Conversely, only the By component was lower in SC 22. The Bz component will have the greatest impact on Earth.

The total variation in the magnetosphere throughout the years from 1944 to 2019 is shown in Figure 3. There were no extraordinary changes in the SCs 18 and 19, while the jump was seen for the Hn parameter in the decreasing phase of the SC 20. The most significant change in all graphs was observed in Hn, and the quietest variation was seen in SC 21. The number of aircraft accidents was lower in this cycle (SC 21), as well. The real abnormalities began after the SC 21; e.g., during the SC 22. The SC 24 was the cycle with the most abnormal variations in all parameters, which contains countless question marks. Is the cause of this abnormal change the Sun, or are other changes occurring on our planet?

5. Conclusion

We would expect a decrease in the number of aircraft accidents with the advancing technology. Nevertheless, the fact that the number of accidents is still high makes it much more likely that these accidents are caused by different effects, e.g., GSs. Considering all the information mentioned above, our study will take an important place in the literature of Air Crash Investigation by examining GSs in detail for the first time, especially in the civil and commercial aviation industry. The latest Airbus incident is the greatest proof of our theory, and unfortunately, this won't be the last. It has been announced that a rare solar flare caused radiation in Earth's atmosphere to spike to the highest levels in nearly 20 years. The solar flare, which was classified as an X5.1, erupted from the AR4274 sunspot on November 11, 2025, and it was followed by a series of milder flares and CMEs that caused aurora display as far south as Florida [17]. After this incident, Airbus ordered immediate software fixes for around 6000 A320-series aircraft [18-19]. This situation is not solely due to design and safety flaws in Airbus's automatic flight control software. Of course, this is one of the most important reasons. However, in addition to this, when we consider that such high-intensity flares occur at specific times, why is their effect much greater at certain times? We believe that this situation coincides not only with solar flares/geomagnetic storms but also with times when there is a change in the components of the Earth's geomagnetic field. We will present a theoretical model using the statistical and observational results as a continuation of our previous studies.

References

[1] Kamide Y.; Chian A.C.L. *Handbook of the solar-terrestrial environment*. Springer-Verlag Publications. 2007, p. 189–220.

[2] Mursula K.; Holappa L.; Lukianova R. Seasonal solar wind speeds for the last 100 years: unique coronal hole structures during the peak and demise of the grand modern maximum. *Geophys. Res. Lett.* 2016, 44(1), p. 30–36.

[3] Demirköz M.B.; Karagöz G.; Kadıoğlu Y.K.; Sözeri H. Vulnerability of economic sectors

to geomagnetic storms and mitigation strategies. *The International Archives of the Photogrammetry, Remote Sensing and Spatial Information Sciences*. Volume XLVIII-M-1-2023 39th International Symposium on Remote Sensing of Environment "From Human Needs to SDGs". 2023, p. 87–94.

[4] Alberti T.; Faranda D.; Consolini G.; de Michelis P.; Donner R.V.; Carbone V. Concurrent effects between geomagnetic storms and magnetospheric substorms. *Universe*. 2022, 8(4), p. 226–244.

[5] Courtillot V.; Gallet Y.; le Mouël J.-L.; Fluteau F.; Genevey A. Are there connections between the Earth's magnetic field and climate? *Earth Planet Sci. Lett.* 2007, 253(3–4), p. 328–339.

[6] Plane Crash Info. www.planecrashinfo.com/. 2022, p. 133.

[7] National Transportation Safety Board. www.ntsb.gov/safety/data/Pages/Data_Stats.aspx. 2022.

[8] Chapman S.C.; McIntosh S.W.; Leamon R.J.; Watkins N.W. Quantifying the solar cycle modulation of extreme space weather. *Geophys. Res. Lett.* 2020, 47(11), p. 1–9.

[9] Aksen U.; Göker Ü.D.; Timoçin E.; Akçay Ç.; İpek M. The effect of geomagnetic storms on aircraft accidents between the years 1919–2023 in civil aviation. *Adv. Space Res.* 2024, 73(1), p. 807–830.

[10] Joshua B.W.; Adamu B.I.; Bonde D.S.; Abbas M.; Adebesin B.O.; Adamu J.L. The relationship between geomagnetic storm and the monthly average temperature. *Equijost*. 2014, 2(1), p. 106–113.

[11] Goddard Space Flight Center. https://omniweb.gsfc.nasa.gov/form/dx2.html. 2025.

[12] ACE Real-Time Solar Wind. www.swpc.noaa.gov/products/ace-real-time-solar-wind. 2025.

[13] Laboratory of Atmospheric and Space Physics. https://lasp.colorado.edu/mms/sdc/public/. 2025.

[14] Time History of Events and Macroscale Intersections During Substorms. https://themis.ssl.berkeley.edu/data_products.shtml. 2025.

[15] GOES Space Environment Monitor. www.ngdc.noaa.gov/stp/satellite/goes/. 2025.

[16] https://www.ncei.noaa.gov/data/goes-space-environment-monitor/access/. 2025.

[17] Rare Solar Flare Caused Radiation in Earth's Atmosphere to Spike to Highest Levels in Nearly 20 Years, Researchers Say. https://www.space.com/astronomy/sun/rare-solar-flare-caused-radiation-in-earths-atmosphere-to-spike-to-highest-levels-in-nearly-20-years-researchers-say. 2025.

[18] Around 6000 Planes Impacted as Airbus Requests Software Update. https://www.newsweek.com/airbus-recall-a320-flight-control-planes-software-11127610. 2025.

[19] American Airlines Says All Planes Impacted by Airbus Glitch Have Been Fixed. https://www.cnbc.com/2025/11/29/airbus-recall-disrupts-global-travel-a320-jets-grounded-glitch-linked-solar-flares.html